



EDUCATIONAL TUTORIAL

A BRIEF INTRODUCTION TO REMOTE SENSING USING GNSS REFLECTIONS

Giulio Ruffini

giulio.ruffini@starlab.es

Research Department, Starlab Barcelona SL

Edifici de l'Observatori Fabra, Camí de l'Observatori, s/n

08035 Barcelona, Spain

Introduction

GNSS-R, the use of Global Navigation Satellite Systems (GNSS) reflected signals is a powerful and potentially disruptive technology for remote sensing: wide coverage, passive, precise, long-term, all-weather and multi-purpose. GNSS emit very precise signals which will be available for decades as part of an emerging infrastructure resulting from the enormous effort invested in GPS, GLONASS, Galileo and augmentation systems. Moreover, GNSS-R technologies will be mature for space applications by the time Galileo and GLONASS are fully deployed, thanks to ongoing ground, air and space research.

In this short tutorial we review the basic concepts of GNSS-R, focusing on marine applications using GPS signal (the pioneering US Global Positioning System).

Global Navigation Satellite Systems

GNSS are designed to provide users with precise position/navigation information. The term “global” navigation refers to the fact that GNSS are to support users everywhere on the surface of the planet, as well as in air and near space. In practice this is achieved with the use of satellite technology. Typically, GNSS satellites are deployed in relatively high orbits and large inclinations to cover most of the globe. For example, GPS satellites have a period of about 12 h and they are located at some 20,000 km altitude in near circular orbits at 55 degrees of inclination (see Table 1). As of today, we have a fully deployed GPS system, a growing GLONASS constellation, and the first successful launch of a Galileo satellite, plus infrastructure on the ground and also on geostationary orbits (so-called augmentation systems).

The principle of operation in GNSS is conceptually straightforward: triangulation based on time of flight of radio signals. The details are rather complex, in fact, as a series of considerations have to be made in order to achieve precise (few m) or ultra precise (few cm) positioning precisions. These include accounting for clock errors, orbit perturbations, atmospheric effects (troposphere, ionosphere) as well as Special and General Relativity effects.

In addition to the space segment, GNSS include a ground

segment as well as so-called augmentation systems, including geostationary satellites providing additional information for a more precise and robust service to dedicated areas.

To see how GNSS work an example will suffice. Let us assume that at a given moment four satellites are in view by a user on the ground, and that the clocks on board the satellites are synchronized. The signals transmitted by each of the satellites contain messages of the sort “I am satellite S in orbit O, and I am transmitting this signal at GPS time T”. It is not hard to see that, upon reception of four such messages, four equations relating the space-time coordinates of the emission and reception events can be written to figure out the user’s time and location. This assumes that the user’s clock, although biased, is precise in the time scales needed to cover the four reception times. It also assumes that the user is capable of inferring the emitter positions using the time and orbit information she gets from the message.

In the next few years, the European Satellite Navigation System (Galileo, with 30 satellites) will be deployed and GPS will be modernized, providing more frequencies and wider bandwidth civilian codes. GLONASS is presently undergoing a revitalization phase, with more and more modern satellites. More than 80 GNSS satellites will soon be emitting precise L-band spread spectrum signals for at least a few decades (see Table 1).

	Operational by	Inclination (degrees)	Number of Planes	Altitude (km)	Signal structure	Number of satellites
GPS	Now	55	6	20,180	CDMA in L1, L2 and L5	29
GLONASS	2010	64.8	3	19,140	FDMA in L1, L2	24
GALILEO	2010	56	3	23,222	CDMA in E5a,b, E6 and E2-L1-E1	30

Table 1. A comparison of GPS, GLONASS and Galileo. Both GPS and Galileo use Code Division Multiple Access (CDMA) to allow all satellite emissions share the same spectral band, while GLONASS uses a frequency division scheme (FDMA). All systems are spread spectrum in L band.

While we address here GNSS-R, other established remote sensing applications using GNSS already exist, including atmospheric sounding for tropospheric water



vapor and ionospheric electron content through refractometric measurements.

GPS emits spread spectrum signals. In simplified form (we focus on the GPS L1 C/A code), the emitted signal $s(t)$ by a given satellite contains three important ingredients: the carrier frequency, the spreading code $CA(t)$ and the actual navigation message $N(t)$ (i.e., “I am satellite S, ... and it is now time T.”). After down-conversion we can describe the received signal in complex form by

$$s(t) = N(t) \cdot CA(t) \cdot e^{i2\pi ft}, \quad (1)$$

where f is the down-converted carrier frequency (which will in general now be Doppler shifted). The spreading code is known and unique for each satellite. The code is a simple series of plus minus ones (a phase modulation of the carrier) at a rate of 1023 “chips” per ms—or about 1 MHz. The Navigation code is again also of the same type, but at a much lower rate of 50 Hz. The details are somewhat tricky, but it is basically possible to “despread” the signal by multiplication (and accumulation during a few ms) of the signal with a signal replica like $s(t+\pi) = CA(t+\pi) \cdot e^{-i2\pi ft}$ with the correct delay and frequency. This makes use of the fact that the navigation code is only shifting at the relatively low rate of once every 20 ms. The “multiply and sum” operation just mentioned—that is, cross-correlation—is typically carried out with data streams of a few ms—while there are no navigation bit transitions. The output of the cross-correlation as a function of the shifting time is a (basically) a triangular pulse with a base of 2 chips (~600 light meters): the cross-correlation waveform shown in Figure 1.

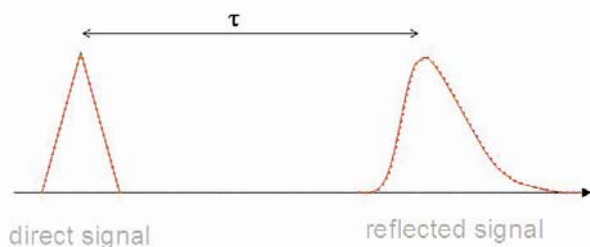


Figure 1. In this figure both the direct and reflected waveforms are illustrated as a function of delay. The direct signal is triangular in shape, while the reflected one is distorted by the reflection process. This transformation, if correctly modeled, can be “undone” in order to compare on the same footing the direct and reflected times of arrival.

GNSS-R

GNSS-R is a form of “passive” radar. “Passive” radar is akin to human sight: our eyes pick up reflected radiation originating from a source like the Sun and decode it to extract information. What we usually call radar will be called here “active radar” to differentiate it from passive radar. Active

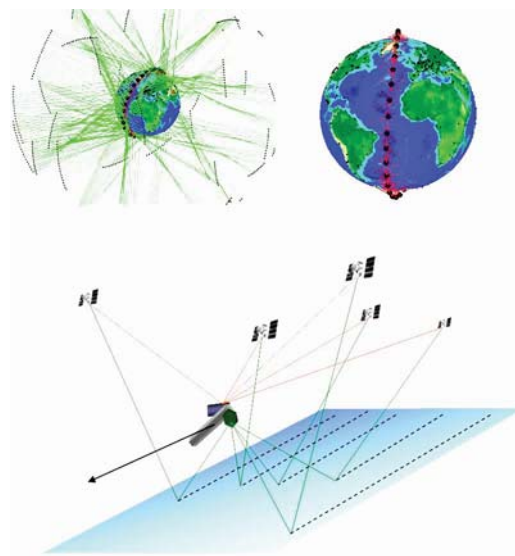


Figure 2. Top, GNSS-R low earth orbiter (LEO) simulation is depicted—one LEO orbit. GNSS satellites are shown as black small dots, with a single LEO receiver. The GNSS satellites emit signals (green) which reflect on the Earth’s surface (the ocean in the figure) and are picked up by the receiver—red lines. The scattering points span an area of scale $\sim 2h$ (where h is the altitude). From space the reflection “ground tracks” provide a comb-like mapping (red arrows) driven by the LEO satellite motion (bottom).

radar is similar to sonar or echo-location, as used by dolphins and bats.

While “passive” bistatic radar has a long history (the first radars were bistatic, i.e., the emitter and receiver were located in separate places with their own antennas), the use of GNSS signals reflected by the sea surface as a remote sensing tool has only generated considerable attention during the last decade, after the pioneering efforts of ESA [Martín-Neira 1993]. Among several, two classes of applications have rapidly emerged in the community: sea-surface altimetry, which aims at retrieving the mean sea level like classical radar altimeters do, and sea-surface reflectometry for the determination of sea roughness and near surface winds.

A key advantage of GNSS-R is its “multistatic” character: unlike monostatic systems, a single receiver will collect information from a simultaneous set of reflection points associated to GNSS emitters (see Figure 2)—typically many more than two. A system in low Earth orbit capable of collecting GPS, Galileo and GLONASS data would potentially be combing the surface with more than twenty reflection tracks at the same time.

Another important aspect is that GNSS signals are very weak as they were not designed for radar applications. For this reason, signal processing plays an important role: although weak, the signals can be detected and contain a wealth of information. The first detection of GNSS signals from space was documented in [Lowe et al., 2002]. More

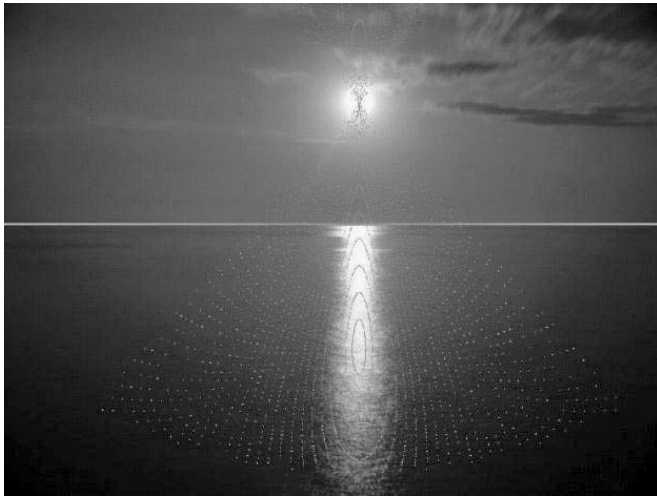


Figure 3. Sun glint over the ocean. The coordinates provide a “tilt-azimuth map”, i.e., for each surface point the facet inclination angles required for the facet to forward the energy towards the camera (receiver). The image intensity as a function of these coordinates can be used to infer the surface roughness. For example, for a rough ocean with large surface slopes, the “glistening zone” will become very large. The use of sun reflections to estimate sea state has a long history (see [Spooner, 1822]).

recently, GPS-R L1 CA signals have been successfully detected from a dedicated experiment in space using a moderate gain antenna [Gleason et al., 2005], complementing a large number of experiments from aircraft and stratospheric balloons, and the resulting data will be used to further validate models.

The reflection process affects the signal in several ways, at the same time degrading (from the point of view of detection) and loading it with information from the reflecting surface. The amplitude is normally reduced, the waveform shape distorted and the coherence mostly lost.

A picture of the sun glint over the ocean will be useful to illustrate these effects—see Figure 3. When the ocean is flat one can see a clear single image reflected on the water from a single point—the specular point (or rather a disk in case of the Sun). For (relatively) short wavelengths the rough ocean can be modeled by facets. Geometric optics can be used to show that the reflected power is proportional to the number of correctly oriented facets and their curvature. The rougher the ocean, the larger the number of facets with large inclination angles will be, providing a wider area of reflection. In GNSS-R, instead of an optical source like the Sun we have GNSS emitters, and instead of a camera we need to build a dedicated GNSS receiver, but the picture is mostly the same. Although the GNSS wavelength (~20 cm) is long compared to the optical, experimental results indicate that Geometric Optics is a reasonably good model in GNSS-R.

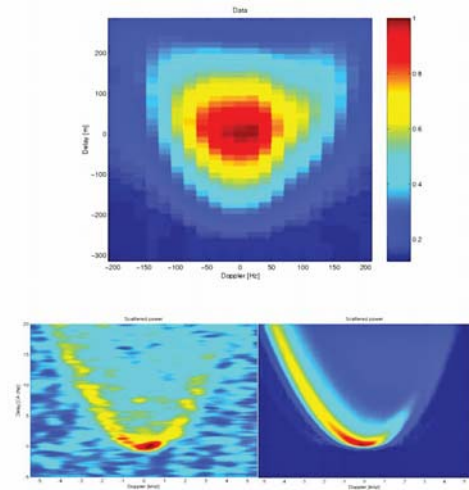


Figure 4. Top: an example DDM as detected from an airborne platform. The scale is arbitrary. The x-axis marks the frequency offset from the specular, while the y-axis displays the delay from the specular. Bottom: GNSS-R DDM data from SSSL's UK DMC space experiment (left) and output from current DDM model in the StarGym simulator (right) [Germain et al., 2005].

Signals scattering from off-specular locations arrive later than the specular—recall that the specular point provides the shortest path. As a function of delay, power will continue to arrive with rather long delays (depending on sea roughness). The waveform will no longer be a triangle. Also, since the ocean surface and scattering geometry evolve in time, the scattered signal will no longer be coherent and will be affected by “speckle”: the resulting electric field sum at the receiver from all the scatterers displays fading phenomena, with the resulting amplitude obeying Rayleigh statistics.

The Delay Doppler Map

At the core of GNSS-R lies the concept of bistatic Delay Doppler mapping. All the information available in the signal is contained in the Complex Delay Doppler map (DDM), correctly referenced in space, time and frequency. The DDM is obtained by cross-correlation of the received signal with a generated “replica” just as we described in Equation (2) but with an important modification. The cross-correlation is computed not only for a range of delays, but also for a range of frequencies, $s(t + \tau) = CA(t + \tau) \bullet e^{-i2\pi(f+\delta f)t}$. For each selected delay and frequency offset value a cross-correlation value is computed.

The received power at different frequency (δf) and delay (τ) offsets can be modeled using the bistatic radar equation [Zavorotny et al., 2000],

$$P_0(\tau, \delta f) = \frac{\lambda^2}{(4\pi)^3} P_t G_{t,A} \int \frac{G_r}{R_r^2 R_t^2} \sigma^0 \chi^2(\tau, \delta f) dS \quad (2)$$

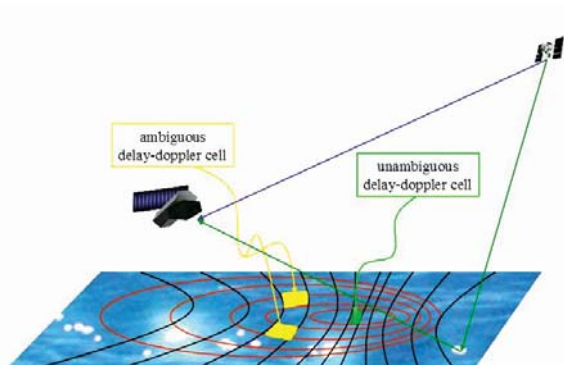


Figure 5. The Delay Doppler map of the surface. The (iso)-Delay ellipses are shown in red, the (iso)-Doppler hyperbolas in black. The direct path from the GNSS satellite to the receiver is shown in blue, while a given reflection path over a scatterer is shown in green. As mentioned in the text, the Delay-Doppler map to the surface is 1 to 2: for a given delay and Doppler, there will in general be two points mapped on the surface (yellow). The exception is the specular (green).

where

- $P_t G_t$ is the Transmitter EIRP (Effective Isotropic Radiated Power),
- A is the Double-way atmosphere attenuation,
- G_r the Receiver antenna gain,
- R_r and R_t are distance between specular point and receiver/transmitter respectively,
- σ^0 is the bistatic scattering coefficient, which in geometric optics at the specular amounts to $R^2/2mss$, where $R=0.61$ (Fresnel coefficient) and mss is the sea-surface mean square slope, depending on the wind speed,
- $\chi^2(\tau, \delta f)$ is the Woodward Ambiguity Function. Tuning delay and frequency has the effect of filtering the power from different reflecting surface regions, as we will describe in some more detail below.

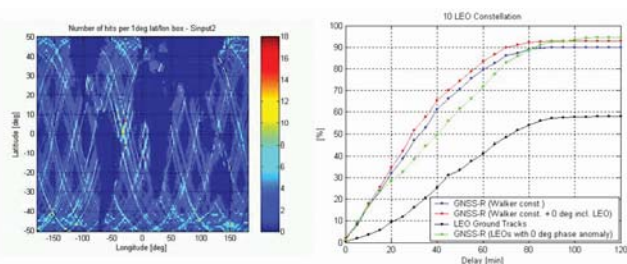


Figure 6. Simulation of a dedicated tsunami monitoring constellation. Left: number of hits per 1 deg lat/lon box after one orbit with 10 GNSS-R satellites after one orbital period. Right, percent of tsunamis detected with a 10 LEO GNSS-R or traditional Radar Altimeters as a function of time after event, showing the clear superiority of the multistatic approach.

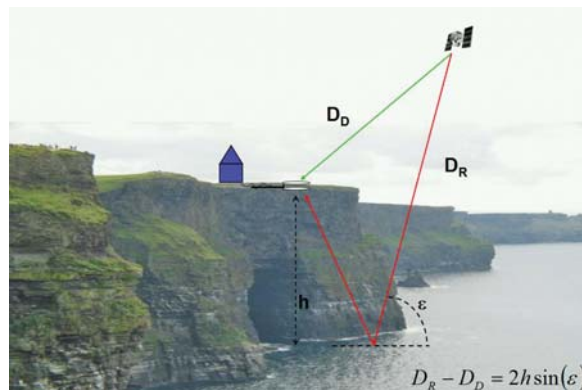


Figure 7. An illustration of coastal altimetry with GNSS-R. The Direct signal travels a shorter path to the antennas than the reflected one. At low altitudes the path difference (in light meters) is proportional to the altitude h over the reflecting surface and the sine of the elevation e .

Figure 4 shows a DDM produced from an air experiment [Germain et al., 2004] and from SSTL’s satellite mission [Gleason et al., 2005], [Germain et al., 2005]. How can this type of plot be interpreted? The first return of the signal originates from the geometric specular point (the one associated to the shortest reflection path). Later returns arise from scattering in (approximate) ellipses around the specular (the intersection of an ellipsoid with the satellites at its focal points with the ocean surface). This provides the “delay” part of the mapping (Figure 1). The Doppler mapping arises from the motion of, e.g., the receiver. Iso-Doppler lines can be approximated by hyperbolas [Caparrini, 1998]—see Figure 5. Thus, selecting a particular frequency offset (Doppler) and delay, filters the power return from selected ocean patches, a process controlled by the Woodward Ambiguity Function described above. Unfortunately the mapping of the surface to Delay Doppler space is not one to one. This means that imaging is not straightforward. Nevertheless, there is quite a bit of information on the DDM, and different techniques can be used to extract information.

Applications in ocean science

The artificial separation between geophysical “layers” (ocean, troposphere, stratosphere, etc.) will disappear in future Earth global models, which will therefore address the fundamental role of atmosphere-ocean coupling in a wide range of spatial and temporal scales. The sea surface provides the ocean-atmosphere link, regulating momentum, energy and gas exchange and several fundamental ocean circulation features which are directly related to wind-wave induced turbulent transports in the oceanic mixed layer. In particular, ocean eddies and gyres are fundamental agents for mixing, heat transport and feedback to general circulation, as well as trans-

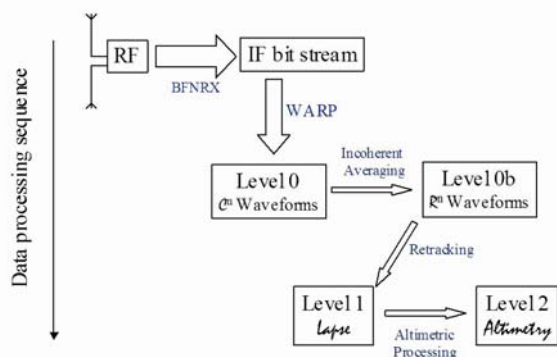


Figure 8. GNSS-R Data processing sequence: from RF data to Altimetry products. Each box represents data processing levels and the arrows processes carried out on the data.

port of nutrients, chemicals and biota for biochemical processes. For this reason, observing this interface appropriately is an important objective for global observation systems, which will require high resolution, wide swaths, frequent revisits and long-term stability. All of these are addressed by the GNSS-R concept.

To statistical first order, the ocean-atmosphere interface is characterized by the local mean sea level (h), significant wave height (SWH) and directional mean square slope (DMSS). Presently, mesoscale measurements of sea surface height constitute an important missing element from the global climate and ocean observation systems. In addition, since ocean forcing is a non-linear and strongly intermittent phenomenon (both in space and time), frequent space-time co-located mesoscale measurements of h and DMSS are highly desirable.

Although GNSS-R cannot provide the precision of dedicated radar altimetry missions, it offers a significant advantage thanks to its multistatic character. The impact of GNSS-R altimetry data to global circulations models has been studied through simulations, with very promising results [Le Traon et al., 2002]. Another recent impact study has focused on the potential of GNSS-R to detect Tsunami's [Martín-Neira et al., 2005]. Major tsunami events occur about once a month, with significant damage reported roughly once a year. Although such events are rare, the higher spatial and temporal resolution available with a GNSS altimeter would provide unprecedented measurements of tsunamis. A dedicated GNSS altimetry system could provide timely warnings, potentially saving many lives. As described in [Soulat et al., 2005], simulations have indicated that a global 100% tsunami detection rate in less than 2 hours is possible with a 10 satellite GNSS-R constellation—see Figure 6.

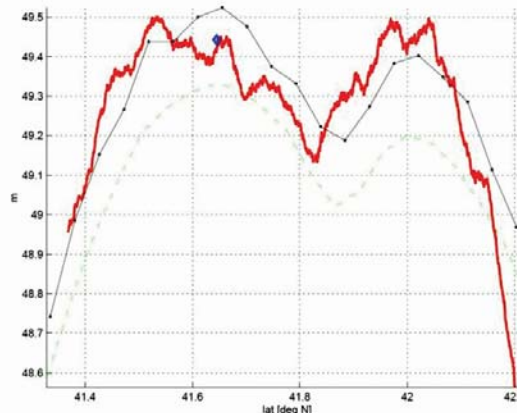


Figure 9. Altimetry results from the Eddy Experiment. The figure shows in red the Sea Surface Height profile obtained processing GPS-R LI data and comparison with Jason-1 altimetry (solid black line) [Ruffini et al., 2004a]. The green dashed line shows the mean sea surface height (also measured by Jason-1).

Altimetry

Altimetry in GNSS-R can be carried out in two general ways, depending on the ranging principle used. In code altimetry the code is used for ranging with the direct and reflected signals. In phase altimetry, the phase is used. All of this is rather similar to normal GNSS processing. The main difference is that the reflected signal is affected by the reflection process, which generally distorts the triangular waveform shape of the return and renders the reflected signal very incoherent. This makes the ranging task rather challenging.

The basic principle in GNSS-R altimetry is that the reflected signal will arrive later than the direct one, since it will travel a longer path to the receiver. The arrival time difference is called the *lapse*. In Figure 7 we illustrate the low altitude reflection process. Uncertainty in the lapse translates rather directly into altimetric uncertainty, $\delta h = \delta l / 2 \sin e$, where e is the local elevation of the satellite at the specular point.

GNSS code ranging with can be conceptualized as radar pulse ranging. Indeed, after correlation with a clean replica, the continuous signal in the CA code can be represented by a triangular pulse. The triangle's base is twice the chip length (300 light meters in GPS CA).

One of the most surprising things about GNSS-R is the fact that the precision attainable is orders of magnitude below the chip length. It is often assumed that the precision obtainable (resolution) in a radar system is of the order of magnitude as the pulse length. For this reason, it is argued, it is impossible that a system like GPS C/A, with a bandwidth of about 1 MHz and associated pulse length of 300 m, can provide centimeter precision ranging. In fact, it can be shown (using the Rao-Cramer bound formalism) that the ranging uncertainty is proportional to the pulse width and inversely proportional to the signal to noise ratio. In practice this

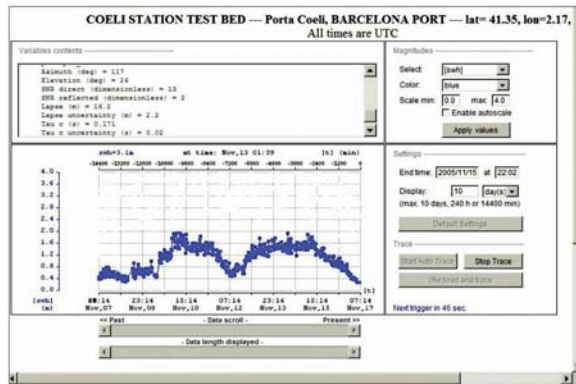


Figure 10. Typical output of a GNSS-R web service (<http://oceanpal.net>), providing sea state information from a coastal location (in this case the Barcelona port).

improvement involves a technique well known to the traditional radar altimetry community: retracking. The term “retracking” itself is a bit of a misnomer. What is involved is simply function-fitting via, e.g., least squares. That is, on reception from a direct or a reflected signal, if a model for the waveform shape is available then precision can be greatly improved by a fitting procedure.

Clearly, retracking is easily carried out with the direct signal, since the shape after correlation is a well-known. With the reflected signal, the scattering process has to be taken into account, and the resulting waveform modeled. The waveform shape, as it happens in monostatic altimetry, is affected in several ways by the reflection process. The peak height is affected, the waveform leading edge modified by the ocean roughness, as is the trailing edge. All these effects can be modeled. Some aspects of the waveform are less sensitive than others to the precise roughness model. The leading edge of the waveform is typically used in GNSS-R altimetry (as is in monostatic altimetry). The entire waveform can be used in the other applications of GNSS-R (as described below).

Code altimetry is robust and applicable for ground, air and space applications. Code altimetry precision from the air has been demonstrated in several experiments [Lowe, 2002]. The term “precision” is used to quantify the noise in a measurement. A measurement can be precise but be biased (inaccurate), or un-precise yet accurate. Accuracy in code altimetry was demonstrated during the airborne Eddy Experiment [Ruffini, et al., 2004a]. In this experiment as in others, two synchronous GPS receivers and antennas were flown. After signal processing to obtain waveforms (Level 0 data, see Figure 8), a geophysical parametric waveform model was used for retracking and estimation of the lapse between the direct and reflected signals with a 1-second precision ranging between 2 and 3 m (Level 1 data), an information then used to estimate the Sea Surface Height along the track (Level 2

data). In that particular experiment, the RMS error of the 20 km averaged GNSS-R absolute altimetric solution with respect to Jason-1 and GPS buoy measurements was of 10 cm, with a 2 cm mean difference (see Figure 9). This first accurate altimetric result provided an important milestone on the road to a GNSS-R mesoscale altimetry space mission.

A few experiments for GNSS-R altimetry based on phase tracking from the ground on coastal locations [Ruffini et al., 2002] or lakes [Treuhaft et al., 2001] have also been performed—obtaining centimeter precisions. Phase processing is severely affected by the ocean roughness and dynamics, however, which render the reflected signal largely incoherent under rough conditions. The coherent power component of the reflected signal is described by $P_c \propto n^2 \bullet \exp[-4\pi(\sigma \sin \epsilon / \lambda)^2]$, where n is the number of scatterers, ϵ the elevation angle, λ the electromagnetic wavelength and σ the sea elevation standard deviation [Beckmann and Spizzichino, 1987]. Clearly, low elevation angles and long electromagnetic wavelengths are needed to work with the coherent component in the open ocean. Several proposed solutions to this problem are under study, e.g., using several frequencies to synthesize longer wavelengths as well as using a filtering approach to recover the coherent part of the signal [Ruffini et al., 2002], or working at low elevation angles [Beyerle et al., 2001][Treuhaft et al., 2005].

Reflectometry and other applications

The scattering of GNSS signals from the ocean can be approximated by an effective Geometric Optics model, where the fundamental physical process is the scattering from facet-like surface elements. The detected GNSS-R return is dominated by the statistics of facet slopes and their curvatures at scales larger than λ . Under a Gaussian assumption, three parameters fully define the detected L-band sea surface slope probability distribution (PDF). These parameters are encapsulated by the directional mean square slope, DMSS, a symmetric tensor which derives from the ocean spectrum at wavelengths larger than λ , and which characterizes the ellipsoidal shape of the slope PDF. DMSS can be extracted from GNSS-R Delay Doppler Maps and optical-sunglint measurements ([Germain et al., 2004], [Cox and Munk, 1954] and [Soulat, 2004]).

Surface slope statistics are related to surface area, and they could help quantify atmosphere-ocean coupling, including momentum, energy and gas fluxes. In addition, L-band sea surface roughness data can be used to support L-band radiometric missions, such as SMOS (Soil Moisture and Ocean Salinity), to both quantify and efficiently separate roughness and salinity contributions to L-band radiometric brightness measurements.

GNSS-R DMSS measurements can complement ocean winds and wave models, and can provide valuable information under extreme conditions such as hurricanes, since L-band is



rain immune. It is possible to relate the DMSS to other quantities, such as surface winds and SWH. However, such relations are indirect and approximate. For example, just as it happens with other instruments (such as radar altimeters), it is possible to have the same mean square slope with very different wind conditions, since the ocean spectrum is not necessarily in equilibrium with the wind at all times. Nevertheless, it may be useful for some applications to produce such approximate products (indicators) related to Sea State and Winds.

An interesting operational application of GNSS-R is coastal monitoring of sea state and tides. From the coast, sea state can be estimated by studying the coherence properties of the reflected signal (see [Soulat et al., 2004a] and Figure 10), while tides can be estimated in coastal areas using code altimetry, or inside harbors using phase methods. Such an instrument can provide a passive, dry alternative to buoys or standard tide gauges.

GNSS-R can also be used to recover estimates of the fraction of new ice and open water in the Arctic. Global observations of sea ice, ice sheets, ice caps, glaciers and their surrounding seas are crucial to determining their mass balance, contributions to sea level change, global circulation and climate change. GNSS-R could be used to develop statistics on the occurrence of such areas in the polar sea ice pack. Other potential measurements include ice altimetry and reflectometry (ice age).

Soil moisture measurements are another potential application currently under study. L-band reflectivity over soil is sensitive to water content, an effect which can be used to quantify soil moisture.

Finally, ionospheric electron density measurements are important for Space Weather research and operations. Data on ionospheric electron content is presently sparse over the oceans, although this situation will be mitigated by occultation measurements. The vertical character of GNSS-R soundings together with their availability over the oceans could fill these gaps.

In conclusion, GNSS-R is a rapidly maturing technology with a niche in applications which require a dense, stable, fast mapping all-weather capability—such as mesoscale altimetry for climate monitoring and operations, hurricane mapping, tsunami detection or sea state monitoring. Relying on present

and future GNSS infrastructures, GNSS-R should provide valuable geophysical measurements for years to come at relatively low cost.

References

1. Beyerle, G. and K. Hoche, "Observation and simulation of direct and reflected GPS signals in radio occultation experiments", *GRL*, 28 (9), 1895-8, May 2001.
2. Beckmann, P., Spizzichino, A., The scattering of electromagnetic waves from rough surfaces, *Atch house, Inc., Nordwood, MA*, 1987
3. Caparrini, M., Using reflected GNSS signals to estimate surface features over wide ocean areas. ESTEC Working Paper No. 2003, Dec 1998.
4. Cox, C., W. Munk, "Measurement of the roughness of the sea surface from photographs of the sun's glitter", *Journal of the Optical Society of America*, 44:838-850, 1954.
5. Garrison, J. L., S. G. Katzberg, M. I. Hill, "Effect of sea roughness on bistatically scattered range coded signals from the Global Positioning System", *GRL*, 25 (13), pp. 2257-60, July 1, 1998.
6. Garrison, J. L., A. Komjathy, V. U. Zavorotny, and S. J. Katzberg, "Wind-Speed Measurement using Forward-Scattered GPS Signals", *IEEE Tran. on Geoscience and Remote Sensing*, 40 (1), 50-65, Jan., 2002.
7. Germain, O., G. Ruffini, F. Soulat, M. Caparrini, B. Chapron, P. Silvestrin, "The Eddy Experiment: GNSS-R specularometry for directional sea-roughness retrieval from low altitude aircraft," *GRL*, 31 (21), Nov. 16, 2004.
8. Germain, O., Caparrini, M., Ruffini, G., First Analysis of SSTL GPS-R experiment, *Starlab Technical Brief TB0012*, May 2005. Available at <http://starlab.es> Library.
9. Le Traon, P.Y., G. Dibarboure, G. Ruffini, E. Cardellach, "Mesoscale Ocean Altimetry Requirements and Impact of GPS-R measurements for Ocean Mesoscale Circulation Mapping," eprint arXiv:physics/0212068, Dec., 2002.
10. Lowe, Stephen T.; LaBrecque, John L.; Zuffada, Cinzia; Romans, Larry J.; Young, Larry E.; Hajj, George A., First spaceborne observation of an Earth-reflected GPS signal, *Radio Science*, Vol. 37, No. 1, 07 February 2002.
11. Martín-Neira, M., A passive reflectometry and interferometry system (PARIS): application to ocean altimetry, *ESA Journal*, vol 17, pp 331-355, 1993.
12. Martín-Neira, M., C. Buck, S. Gleason, M. Unwin, M. Caparrini, E. Farrès, O. Germain, G. Ruffini and F. Soulat, "Tsunami detection using the PARIS concept", *Progress in Electromagnetics Research Symposium 2005, Hangzhou, China, August 22-26*.
13. Ruffini G., M. Caparrini, L. Ruffini, PARIS Altimetry with L1 Frequency Data from the Bridge 2 Experiment, *Abridged Starlab ESA/ESTEC Technical Report-no: ESA/ESTEC Contract No. 14285/85/nl/pb, Starlab CCN3-WP3, Dec 2002*. Available at <http://starlab.es> Library.
14. Ruffini, G., F. Soulat, M. Caparrini, O. Germain, Martín-Neira, "The eddy experiment - accurate GNSS-R ocean altimetry from low altitude aircraft," *GRL*, 31 (12), June 18, 2004.
15. Soulat, F., M. Caparrini, O. Germain, P. Lopez-Dekker, M. Taani, G. Ruffini, "Sea state monitoring using coastal GNSS-R," *GRL*, 31 (21), Nov. 5, 2004a.
16. Soulat, F., "Sea Surface Remote Sensing with GNSS and Sunlight Reflections", Ph.D. Dissertation, *Universitat Politècnica de Catalunya*, 2004b.
17. Soulat, F., M. Caparrini, O. Germain, G. Ruffini, "PARIS Mission Impact Analysis," *GNSS Reflections Workshop 2005, Surrey, UK, June, 2005*. Available at <http://starlab.es> Library.
18. Spooner, J., Sur la lumiere des ondes de la mer, *Corresp. Astronomique du Baron de Zach*, 6:331, 1822.
19. Treuhaft, R. N., S. T. Lowe, C. Zuffada, Y. Chao, "Two-cm GPS altimetry over Crater Lake", *GRL*, 28 (23), pp. 4343-6, Dec. 1, 2001.
20. Treuhaft, R., S. Lowe, E. Cardellach, G. Franklin, T. Meehan, L. Young, "Coastal Altimetry and Atmospheric Inhomogeneities from Reflected GPS Signals," *GNSS Reflections Workshop 2005, Surrey, UK, June, 2005*.
21. Zavorotny, V.U., Voronovich, A.G., (2000), Scattering of GPS Signals from the Ocean with Wind Remote Sensing Application, *IEEE Transactions on Geoscience and Remote Sensing*, Vol. 38, No. 2, pp. 951-964.

IEEE

GEOSCIENCE *and* REMOTE SENSING

Newsletter



<http://www.grss-ieee.org/menu.taf?menu=Publications&detail=newsletter>

Editor: Adriano Camps

